Biosensors and Bioelectronics 74 (2015) 150–155

Contents lists available at ScienceDirect

Biosensors and Bioelectronics

journal homepage: www.elsevier.com/locate/bios

Integrated OLED as excitation light source in fluorescent lateral flow immunoassays

Vishak Venkatraman, Andrew J. Steckl *

Nanoelectronics Laboratory, University of Cincinnati, Cincinnati, OH 45221-0030, USA

ARTICLE INFO

Article history:
Received 19 April 2015
Received in revised form
16 June 2015
Accepted 19 June 2015
Available online 20 June 2015

Keywords:
Lateral flow
Immunoassay
OLED
Quantum dot
Integration
Limit of detection

ABSTRACT

The integration of organic light emitting diodes (OLEDs) as excitation light sources for quantum dot-based fluorescent lateral flow immunoassay systems (LFIA) was investigated. This approach has the potential to deliver a sensitive visible detection scheme for low-cost, disposable lab-on-chip point-of-care (POC) diagnosis system. Thin film phosphorescent green OLEDs fabricated on plastic substrates were integrated on-chip to excite the test line of a quantum dot-based LFIA (QD-LFIA). OLEDs were fabricated by sequential deposition of organic thin films (total of ~100 nm) onto ITO-coated PET substrates. CdSe/ZnS QDs emitting at 655 nm and Au nanoparticles (NP – 10 nm size) conjugated antibodies were used for the fluorescence QD-LFIA and conventional reflection-mode Au NP-LFIA, respectively. Thin plastic color light filters were integrated for filtering the excitation light source and, thereby, increasing the contrast of the emitted light for optimized visual detection. Integration of the OLED and color filters with the analytical membrane was achieved using adhesive techniques facilitated by the planar nature of the layers, which suggests possible large scale manufacturing using roll-to-roll processing. Gray scale analysis from digital images captured with a digital camera was used to quantify the visual sensitivity. The signal intensity, signal-to-noise ratio (SNR) and the limit of detection (LOD) of OLED integrated QD-LFIAs were compared to Au NP LFIAs. OLED QD-LFIA exhibited superior performance in all signal aspects: 7–8 × higher signal intensity and SNR, and a 7 × lower LOD of 3 nM (measured at $S/N=3$). These results demonstrate the potential of OLED-integrated in LFIA devices for obtaining sensitive, fast and low-cost POC diagnostics.

1. Introduction

Lab-on-chip (LOC) concepts have provided a successful path for the development of low-cost and disposable point of care diagnostic (POC) devices. LOC focuses on ways to miniaturize laboratory scale equipment to perform diagnosis on a small scale, thereby making the system cheap and portable. Microfluidics is the key underlying technology that enables miniaturizing of many LOC diagnostic devices (Haeberle and Zengerle, 2007; Roman and Kennedy, 2007; Yager et al., 2006; Yi et al., 2006). Paper-based devices are currently being investigated (Steckl, 2013; Tobjörk and Österbacka, 2011) for a variety of applications such as electronics, displays and sensors because of the inherent low cost of the material and of roll-to-roll manufacturing. Microfluidic devices that use capillary transport in paper represent a very attractive and surprisingly versatile path for low cost LOC devices (Fu et al., 2011; Martinez et al., 2009; Parolo and Merkoçi, 2013; Yager et al., 2006). Immunochromatographic assays, also known as lateral flow immunoassays (LFIA), use capillary wicking for the transport of analytes to the detection zone where the immunoreaction takes place (Ngom et al., 2010; Posthuma-Trumpie et al., 2009). The inherent capillary pump action integrated in the diagnostic device removes a major drawback of polymer (such as PDMS, PMMA or PC) based microfluidics devices, which normally require external pumps for fluidic transport and manipulation (Yetisen et al., 2013). In addition to their low cost, LFIA devices operate rapidly (Yetisen et al., 2013), with the detection of the analyte performed in a few minutes. The outcome of the immunoreaction can give a simple qualitative ("yes/no") answer in nature (Posthuma-Trumpie et al., 2009). Many such assays commonly use colloidal gold (Hirsch et al., 2003; Kolosova et al., 2007; Krska and Molinelli, 2009; Kusano et al., 2007; Ngom et al., 2010; Posthuma-Trumpie et al., 2009; Verheijen et al., 1998) nanoparticles (Au NP), which when accumulated in the test line region of the LFIA appear reddish in color and thereby giving a qualitative visual readout for the presence of analyte. A widely utilized commercial Au NP-LFIA is the pregnancy test strip, which detects human chronic gonadotropin (hCG) hormones in urine specimens (Tanaka et al., 2006). Multiple

* Corresponding author.
E-mail address: a.steckl@uc.edu (A.J. Steckl).

http://dx.doi.org/10.1016/j.bios.2015.06.049
0956-5663/

commercial products use Au NPs as the label for hCG pregnancy tests.

The use of fluorescent particles in these assays (Bamrungsap et al., 2014; Corstjens et al., 2008; Gui et al., 2014; Xia et al., 2009) has recently gained considerable interest due to the resulting high LFIA sensitivity (Xie et al., 2014). Quantum dot (QD) fluorescent particles, owing to their high photoluminescence properties (Lu et al., 2003), as well as colloidal water soluble synthesis methods (He et al., 2007), are being increasingly explored in medical applications (Cui et al., 2008; Han et al., 2001; Li et al., 2010b; Montón et al., 2012; Taranova et al., 2015; Zhang et al., 2009). Recently, QDs have received attention for incorporation into LFIA devices. Syphilis detection using QD-LFIA reported by Yang et al. (2010) has shown 10× improvement in visual limit-of-detection (LOD) by using QDs over conventional Au NP-based system. Similar improvement of visual sensitivity, were reported by Li et al. (2010a) in detecting human ceruloplasmin. Quantitative measurements were performed (Li et al., 2010a) with the QD-LFIA using an external reader unit. These results show the potential of fluorescent particles as visual indicators in LFIA devices. However, these LFIA systems also require separate readers with light sources and detectors, usually benchtop units that are not easily portable and thus harder to use in POC applications.

Organic light emitting diodes (OLED) consist of a series of thin films of various organic materials deposited on substrates, resulting in devices that emit and detect light when biased (Tang and VanSlyke, 1987). While OLEDs are usually formed on glass substrates, the fact that the thin film deposition takes place at relatively low temperatures makes it possible to fabricate them on plastic films or paper substrates (Purandare et al., 2014; Zocco et al., 2014). This facilitates integration with LFIAs for realizing LOC applications (Williams et al., 2014) for medical diagnostics. OLEDs have several advantages compared to their inorganic counterparts (LED), including physical flexibility and large area fabrication capability (Williams et al., 2014). Fluorescence detection in plastic microfluidic chips using separate OLED excitation has been reported by Pais et al. (2008) to exhibit sensitive detection (100 nM). However, a system that integrates OLED with paper microfluidic devices has not been realized yet. Such an integrated system would take the advantage of both paper-based diagnostics as well and the potential of organic optoelectronic devices.

In this manuscript, we explore the integration of OLEDs as the excitation source in QD-LFIA devices for high sensitivity, visual observation-based qualitative LFIA diagnosis. Red emitting (655 nm) QDs were used as fluorophores in the LFIA. Though these QDs have maximum absorption in the UV/blue region, the higher efficiency and brightness of green OLEDs compared to blue OLEDs, led us to choose the former. To enhance the visual signal from the QDs in the test line of the LFIA, two color filters were also incorporated in the device. Fig. 1 shows an overall sketch of the integration concept.

The QD-LFIA was compared with conventional Au NP-based LFIA operated under similar conditions in order to ascertain improvements in contrast and LOD. A high sensitivity system will improve the LOD in several LFIA systems that provide qualitative (i.e. yes/no) analysis, such as home pregnancy test kits and flu kits.

2. Materials and methods

2.1. OLED fabrication

A phosphorescence based green emitting OLED stack, ITO/NPB/CBP:Ir/BCP/ALQ3/LiF/Al, was chosen due to its inherent high efficiency and brightness, as demonstrated by the Forrest group (Adachi et al., 2001). Energy levels of the organic layers stack are shown in Fig. 2a.

OLEDs were fabricated on ITO-coated PET sheets (5 mil) having a sheet resistance of 60 Ω/square (Sigma Aldrich). To facilitate ease of fabrication, PET sheets were attached to rigid glass substrates before processing. The fabrication process starts by lithographically patterning the ITO to produce 4 mm wide strips. After ITO patterning, the surface was cleaned using O_2 plasma (250 W power) for 2 min. The substrates were then transferred to a high vacuum deposition system and the organic layers were sequentially deposited through a shadow mask at an operating pressure of 5×10^{-7} Torr. The thickness of the total organic stack was ~100 nm. Next, the substrates were very briefly removed to load the anode mask. Lithium fluoride (LiF) and aluminum were then deposited (total of ~40 nm) in the vacuum system, forming the anode electrode in devices with an active area of 4 mm × 4 mm. After the OLED fabrication was completed, the PET sheet was removed from the glass substrate in order to integrate the OLED with the LFIA. Each OLED substrate measured 15 mm × 15 mm, as shown in Fig. 2b. It is important to note that in these bottom-emitting OLEDs, the emission that is utilized in the overall device propagates through ITO layer and the PET sheet.

OLED current–voltage (*I–V*) characteristics were obtained with

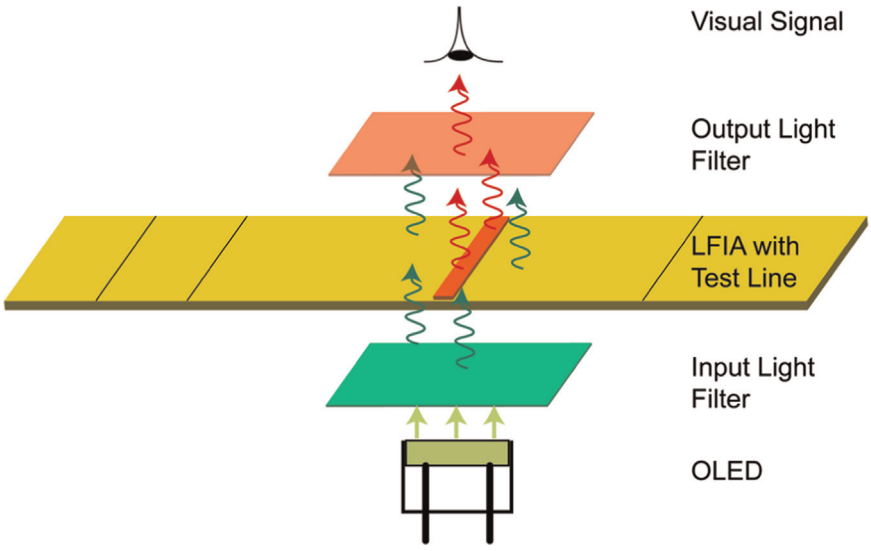

Fig. 1. Schematic of OLED/LFIA integration approach.

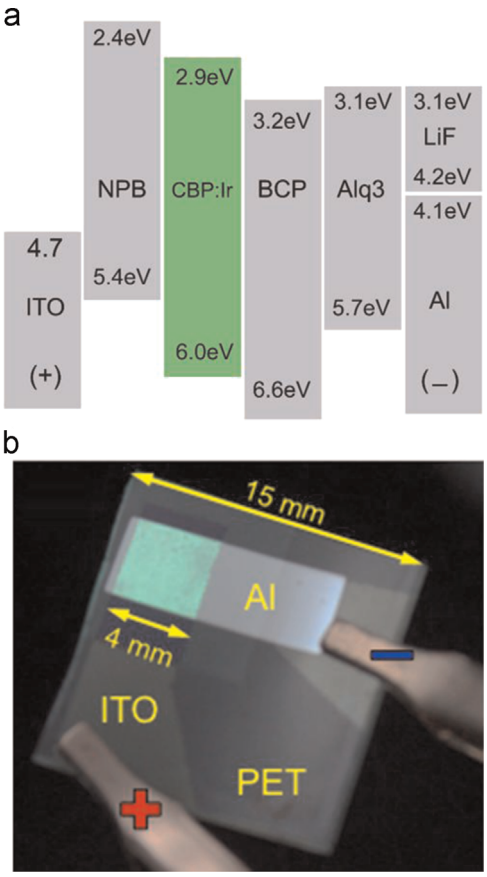

Fig. 2. OLED details: (a) constituent layers and their respective HOMO/LUMO energy levels; (b) photo of emitting green OLED pixel on a PET substrate.

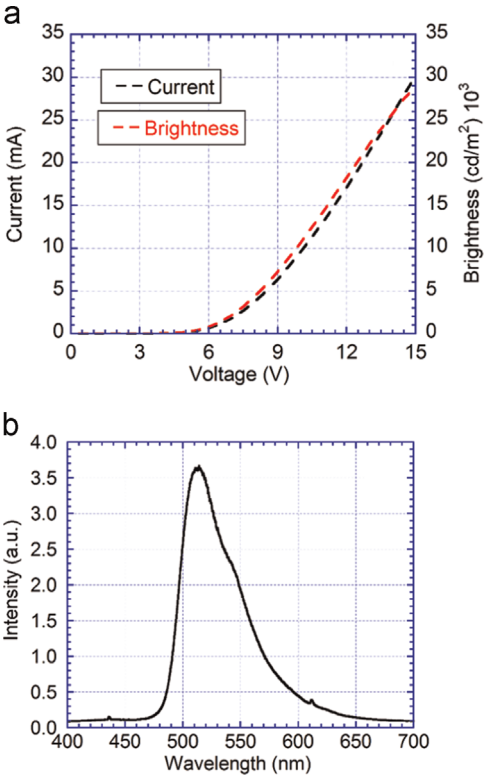

Fig. 3. OLED characteristics: (a) current and brightness vs. voltage; (b) emission spectrum.

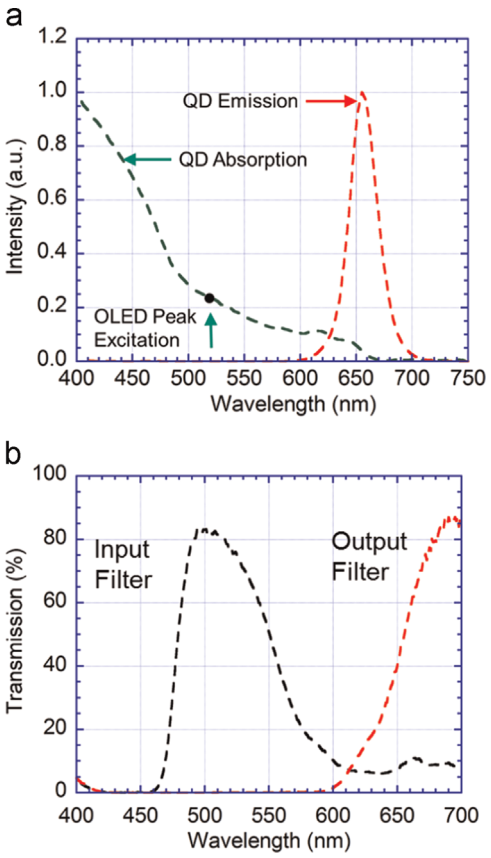

Fig. 4. Optical spectra of the components of the integrated OLED/QD-LFIA device: (a) absorption and emission spectra of quantum dots. OLED peak excitation wavelength also indicated; (b) transmission of green and red filters.

a variable voltage source in steps of 0.5 V with current values recorded by an HP-6634B DC power source. Brightness was measured using a luminance meter (Konica-Minolta CS-200). The spectral output was obtained using Ocean Optics SD 2000 spectrometer. Fig. 3 shows an example of current–voltage–brightness and spectral characteristics of the OLEDs fabricated.

2.2. LFIA fabrication

A simple immunoreaction-based fluorescent lateral flow assay was chosen to evaluate the performance of the OLED-integrated LFIA device. The capture mechanism is based on antibody–antibody reaction rather than using a specific analyte to form a sandwich assay. The analytical membrane with test lines (Meridian Biosciences Inc.) measured 60 mm × 6 mm. The quantum dot fluorophore conjugate, Donkey Anti-Mouse QD 655 (Life Technologies) binds to the test lines present in the analytical membrane. Fig. 4a shows the absorption and emission spectra measured using the Nanodrop instrument (Thermo Scientific). Two thin plastic light filters were integrated in the device to improve the contrast and produce a higher visual sensitivity: an input green filter (to reduce the red component in the OLED emission spectrum) and an output red filter (to remove green OLED emission after QD excitation). As can be seen from Fig. 3b, the OLED has a long emission tail into the red spectrum, with some emission at ~600 to 620 nm, which competes with the red emission signal from the test line. To reduce the red component, a green light filter (Chroma Green, Rosco Laboratories), was used as the *input* light filter. The spectral shaping is shown in Fig. 5a. The *output* red filter (Medium Red, Rosco Laboratories) was used to eliminate the green light from the OLED source, and allow only the light from the QDs,

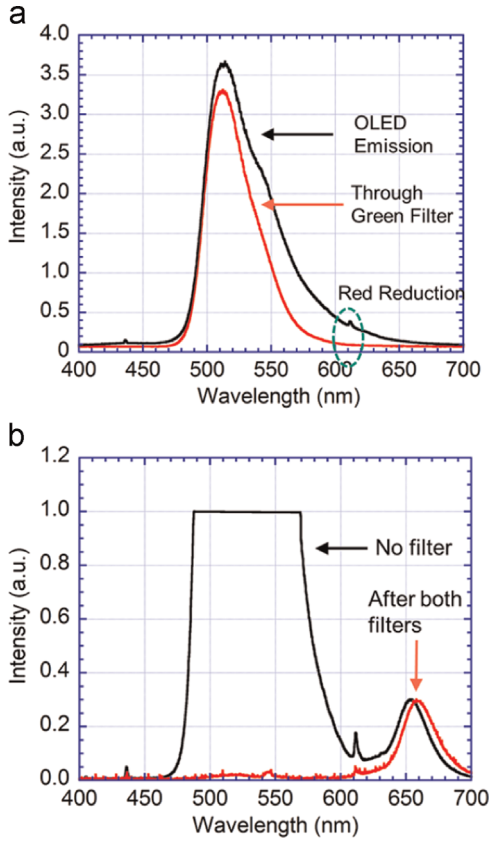

Fig. 5. Spectral response showing the effect of light filters in the OLED/LFIA device: (a) OLED emission through input light filter; (b) OLED+QD emission through input and output light filter.

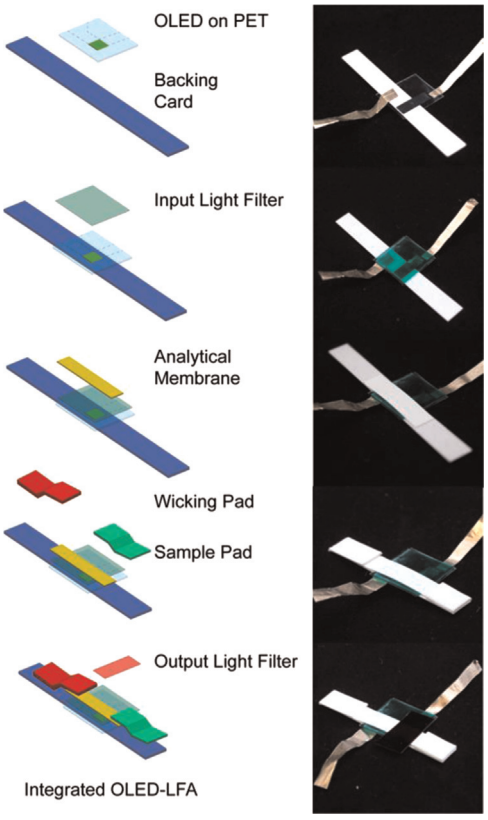

Fig. 7. Fabrication steps of integrated OLED/LFIA device.

which emit in the deep red region (655 nm) as seen in Fig. 5b. The LFIA was constructed by attaching the analytical membrane to a backing card, and attaching the sample and wicking pads (Diagnostic Consulting Network Inc.) to the two ends of membrane, with an overlap of ~5 mm. The sample and wicking pads measured 20 mm × 6 mm. The assay was performed by dipping the LFIA into conjugated QD solutions of various concentrations for a specific amount of time. For conventional Au-NP LFIA, Donkey Anti-Mouse Au solution (Abcam) was used to perform assays under the same conditions as the QD solution. Fig. 6 illustrates the basic operation of the LFIA and the capture lines under UV excitation.

2.3. Integration

Fig. 7 illustrates the integration process of the OLED with the QD-LFIA device. The integration starts by attaching the OLED fabricated on PET onto an adhesive backing membrane (DCN). Copper tapes were attached to the OLED to provide external electrical contact. The input (green) plastic filter is then placed on top of the OLED. Next, the analytical membrane is placed on top of the OLED and color filter and aligned such that the position of the test line lies within the device emission area. Adhesives were used

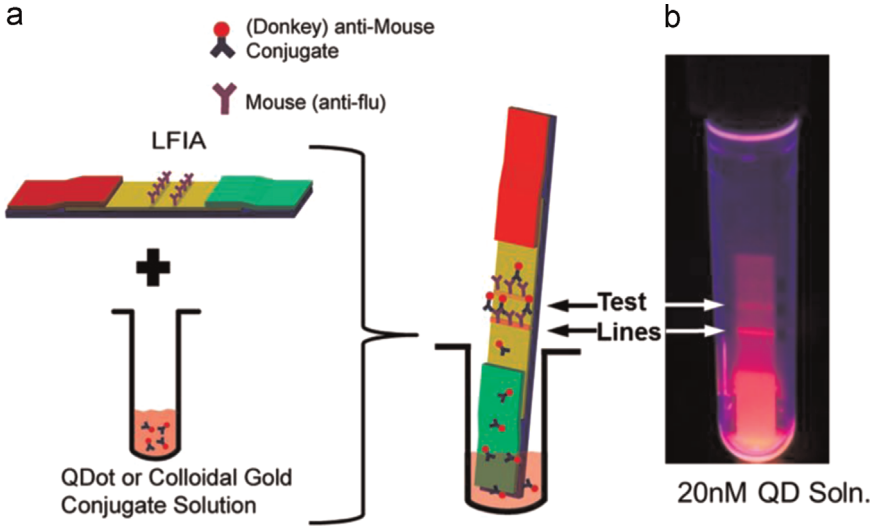

Fig. 6. LFIA working principle: (a) dipstick assay format; (b) UV excitation after assay process shows emission from QDs captured on test lines.

between these layers for attachment. The sample and wicking pads were then attached to the analytical membrane for enabling the lateral fluid flow. Finally, the output (red) filter is attached on top of the test line region.

The effect of attaching adhesive-backed plastic sheets to the LFA membrane (by room temperature lamination) was investigated by comparing the flow of water to that in conventional membranes. No significant differences were observed in the liquid front and flow rate between the two cases.

3. Results and discussion

The assays were performed by inserting the LFIA unit into a 100 μL QD solution of varying concentrations for 10 min. For comparison, the same procedure was used with Au-NP solution at the same concentration and duration. A uniform drying process was used for both assays. Fig. 8a shows the resulting comparison using photographs under room light conditions of the two types of LFIAs at 100 nM concentration. The signal generated by the QD-LFIA is much more visible than that from the Au-NP LFIA, with the QD test line being much brighter and sharper than the NP test line. To make the comparison complete, a QD-LFIA with no OLED excitation is also shown. To quantify the contrast, gray line scans were taken (Image J software) in the test line region. The corresponding data is plotted in Fig. 8b. The signal from the QD-LFIA is seen to be ~5× larger than from the Au-NP based device. This clearly indicates superior sensitivity of visual detection for the OLED integrated QD-LFIA.

Assays at various concentrations were used to determine the LOD in the two cases. In all cases, the OLED was biased at the same voltage and the same room lighting conditions were used. Signal-to-noise (S/N) ratios were calculated from the Image J data as follows. Gray scale pixel values in the test line region were averaged and the difference from the average of the background pixel gray values (around the test line region) was calculated. This difference is taken as the signal intensity. The signal is plotted in Fig. 9a as a function of conjugate concentration. As indicated by the dashed lines, the sensitivity (i.e. change in signal with change in concentration) in the linear region is ~8 to 9× higher for the QD-LFIA. While both device types experience some saturation at the higher concentration, the effect is more pronounced for the Au-NP device. The noise intensity was taken as the average of the difference between consecutive gray pixel values in the Image J line scan away from the test line. The S/N ratio is then given by the ratio between the signal and noise intensities. Fig. 9b shows the S/N ratio for both QD-LFIA and Au NP-LFIA at various conjugate concentrations. A S/N ratio of 3 was chosen to represent the LOD condition, which was reached at 3 nM for the integrated QD-LFIA and at 21 nM for Au-based LFIA.

While the results of the OLED/QD-LFIA in Fig. 9 are obtained with individual devices, several fabrication runs of OLED/LFA devices were performed in order to obtain preliminary information on reproducibility of our results. A total of 14 tests were performed using either 10 or 30 nM QD concentration. The signal range for all tests (at either concentrations) was ± 16%. These results indicate reasonable reproducibility for these initial efforts. Clearly, improvements will be required before the next step in the development of devices for clinical testing.

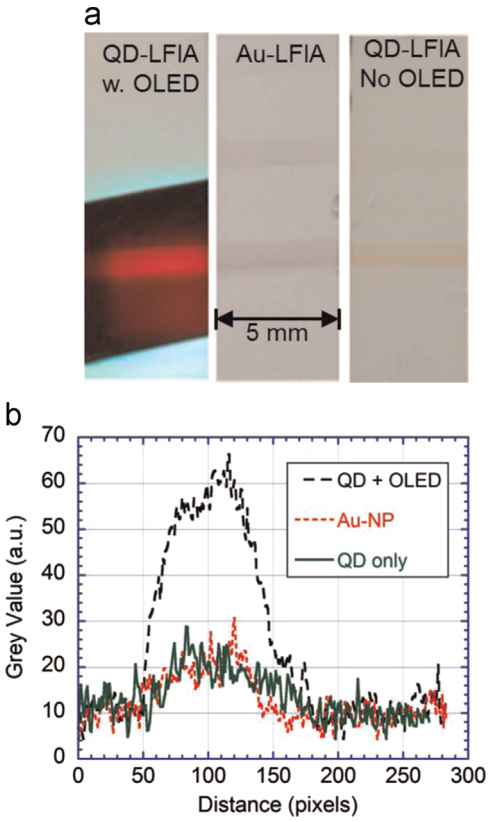

Fig. 8. Comparison of LFIA operation-emissive integrated OLED-QD approach vs. reflective Au-NP approach: (a) side-by-side photos of the QD LFIA with and without OLED excitation and Au-NP LFIA; (b) equivalent gray scale contrast comparison.

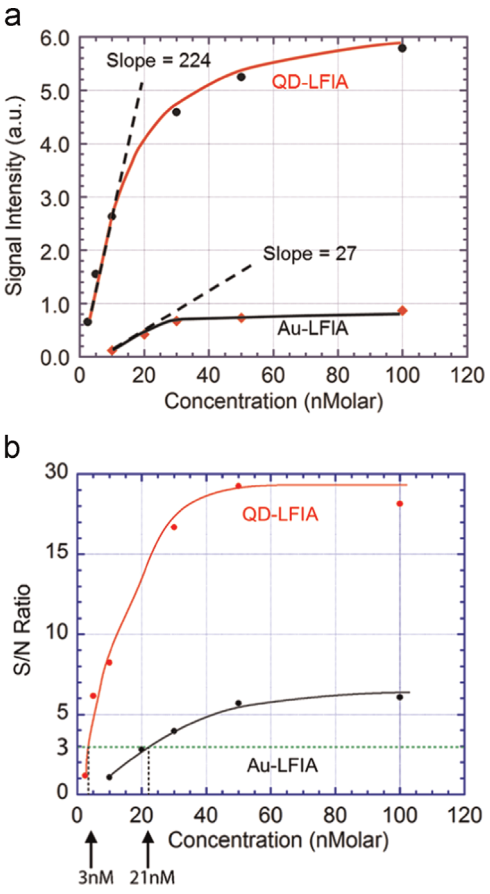

Fig. 9. Visual characteristics of QD and Au NP-LFIA as a function of concentration of conjugate solution: (a) signal intensity; dashed lines indicate signal sensitivity in linear region; (b) signal-to-noise ratio; LOD concentrations indicated by the arrows were taken at SNR=3.

4. Summary

In summary, the integration of OLED-based excitation of QD fluorescent labels in LFIA devices was demonstrated. Integration was achieved by attaching OLEDs fabricated on PET with color plastic filters and the LFIA components. QD-based fluorescent LFIAs were used for proof of concept and visual sensitivity was compared to that of conventional Au NP-based LFIA. A significant improvement in signal intensity, contrast and limit-of-detection was achieved in integrated OLED devices compared to conventional LFIA. The LOD for OLED-excited QD-LFIA was ~3 nM compared to 21 nM for the conventional LFIA, or a 7× improvement. Combined with other attractive factors of LFIA and OLEDs, such as low cost and large-scale roll-to-roll manufacturability, these results show that integrating OLEDs in paper-based diagnostic system is a high potential path for lab-on-chip device applications.

Acknowledgments

The authors gladly acknowledge funding from NSF (ENG-1236987) USA and technical discussions and support from K. Kozak (Meridian Biosciences Inc.)

References

Adachi, C., Baldo, M.A., Thompson, M.E., Forrest, S.R., 2001. Nearly 100% internal phosphorescence efficiency in an organic light-emitting device. J. Appl. Phys. 90 (10), 5048–5051.
Bamrungsap, S., Apiwat, C., Chantima, W., Dharakul, T., Wiriyachaiporn, N., 2014. Rapid and sensitive lateral flow immunoassay for influenza antigen using fluorescently-doped silica nanoparticles. Microchim. Acta 181 (1–2), 223–230.
Corstjens, P.L., van Lieshout, L., Zuiderwijk, M., Kornelis, D., Tanke, H.J., Deelder, A. M., van Dam, G.J., 2008. Up-converting phosphor technology-based lateral flow assay for detection of Schistosoma circulating anodic antigen in serum. J. Clin. Microbiol. 46 (1), 171–176.
Cui, D., Pan, B., Zhang, H., Gao, F., Wu, R., Wang, J., He, R., Asahi, T., 2008. Self-assembly of quantum dots and carbon nanotubes for ultrasensitive DNA and antigen detection. Anal. Chem. 80 (21), 7996–8001.
Fu, E., Ramsey, S., Kauffman, P., Lutz, B., Yager, P., 2011. Transport in two-dimensional paper networks. Microfluid Nanofluid 10 (1), 29–35.
Gui, C., Wang, K., Li, C., Dai, X., Cui, D., 2014. A CCD-based reader combined with CdS quantum dot-labeled lateral flow strips for ultrasensitive quantitative detection of CagA. Nanoscale Res. Lett. 9 (1), 1–8.
Haeberle, S., Zengerle, R., 2007. Microfluidic platforms for lab-on-a-chip applications. Lab Chip 7 (9), 1094–1110.
Han, M., Gao, X., Su, J.Z., Nie, S., 2001. Quantum-dot-tagged microbeads for multiplexed optical coding of biomolecules. Nat. Biotechnol. 19 (7), 631–635.
He, R., You, X., Shao, J., Gao, F., Pan, B., Cui, D., 2007. Core/shell fluorescent magnetic silica-coated composite nanoparticles for bioconjugation. Nanotechnology 18 (31), 315601.
Hirsch, L., Jackson, J., Lee, A., Halas, N., West, J., 2003. A whole blood immunoassay using gold nanoshells. Anal. Chem. 75 (10), 2377–2381.
Kolosova, A.Y., De Saeger, S., Sibanda, L., Verheijen, R., Van Peteghem, C., 2007. Development of a colloidal gold-based lateral-flow immunoassay for the rapid simultaneous detection of zearalenone and deoxynivalenol. Anal. Bioanal. Chem. 389 (7–8), 2103–2107.
Krska, R., Molinelli, A., 2009. Rapid test strips for analysis of mycotoxins in food and feed. Anal. Bioanal. Chem. 393 (1), 67–71.
Kusano, N., Hirashima, K., Kuwahara, M., Narahara, K., Imamura, T., Mimori, T., Nakahira, K., Torii, K., 2007. Immunochromatographic assay for simple and rapid detection of Satsuma dwarf virus and related viruses using monoclonal antibodies. J. Gen. Plant Pathol. 73 (1), 66–71.
Li, Z., Wang, Y., Wang, J., Tang, Z., Pounds, J.G., Lin, Y., 2010a. Rapid and sensitive detection of protein biomarker using a portable fluorescence biosensor based on quantum dots and a lateral flow test strip. Anal. Chem. 82 (16), 7008–7014.
Li, Z., Huang, P., Lin, J., He, R., Liu, B., Zhang, X., Yang, S., Xi, P., Zhang, X., Ren, Q., 2010b. Arginine–glycine–aspartic acid-conjugated dendrimer-modified quantum dots for targeting and imaging melanoma. J. Nanosci. Nanotechnol. 10 (8), 4859–4867.
Lu, W., Ji, Z., Pfeiffer, L., West, K., Rimberg, A., 2003. Real-time detection of electron tunnelling in a quantum dot. Nature 423 (6938), 422–425.
Martinez, A.W., Phillips, S.T., Whitesides, G.M., Carrilho, E., 2009. Diagnostics for the developing world: microfluidic paper-based analytical devices. Anal. Chem. 82 (1), 3–10.
Montón, H., Roldán, M., Merkoçi, A., Rossinyol, E., Castell, O., Nogués, C., 2012. The use of quantum dots for immunochemistry applications. In: Soloviev, M. (Ed.), Nanoparticles in Biology and Medicine. Humana Press, United States, pp. 185–192.
Ngom, B., Guo, Y., Wang, X., Bi, D., 2010. Development and application of lateral flow test strip technology for detection of infectious agents and chemical contaminants: a review. Anal. Bioanal. Chem. 397 (3), 1113–1135.
Pais, A., Banerjee, A., Klotzkin, D., Papautsky, I., 2008. High-sensitivity, disposable lab-on-a-chip with thin-film organic electronics for fluorescence detection. Lab Chip 8 (5), 794–800.
Parolo, C., Merkoçi, A., 2013. Paper-based nanobiosensors for diagnostics. Chem. Soc. Rev. 42 (2), 450–457.
Posthuma-Trumpie, G.A., Korf, J., van Amerongen, A., 2009. Lateral flow (immuno) assay: its strengths, weaknesses, opportunities and threats. A literature survey. Anal. Bioanal. Chem. 393 (2), 569–582.
Purandare, S., Gomez, E.F., Steckl, A.J., 2014. High brightness phosphorescent organic light emitting diodes on transparent and flexible cellulose films. Nanotechnology 25 (9), 094012.
Roman, G.T., Kennedy, R.T., 2007. Fully integrated microfluidic separations systems for biochemical analysis. J. Chromatogr. A 1168 (1), 170–188.
Steckl, A.J., 2013. Circuits on cellulose. Spectr. IEEE 50 (2), 48–61.
Tanaka, R., Yuhi, T., Nagatani, N., Endo, T., Kerman, K., Takamura, Y., Tamiya, E., 2006. A novel enhancement assay for immunochromatographic test strips using gold nanoparticles. Anal. Bioanal. Chem. 385 (8), 1414–1420.
Tang, C., VanSlyke, S., 1987. Organic electroluminescent diodes. Appl. Phys. Lett. 51 (12), 913–915.
Taranova, N., Berlina, A., Zherdev, A., Dzantiev, B., 2015. 'Traffic light' immunochromatographic test based on multicolor quantum dots for the simultaneous detection of several antibiotics in milk. Biosens. Bioelectron. 63, 255–261.
Tobjörk, D., Österbacka, R., 2011. Paper electronics. Adv. Mater. 23 (17), 1935–1961.
Verheijen, R., Stouten, P., Cazemier, G., Haasnoot, W., 1998. Development of a one step strip test for the detection of sulfadimidine residues. Analyst 123 (12), 2437–2441.
Williams, G., Backhouse, C., Aziz, H., 2014. Integration of organic light emitting diodes and organic photodetectors for lab-on-a-chip bio-detection systems. Electronics 3 (1), 43–75.
Xia, X., Xu, Y., Zhao, X., Li, Q., 2009. Lateral flow immunoassay using europium chelate-loaded silica nanoparticles as labels. Clin. Chem. 55 (1), 179–182.
Xie, Q.-Y., Wu, Y.-H., Xiong, Q.-R., Xu, H.-Y., Xiong, Y.-H., Liu, K., Jin, Y., Lai, W.-H., 2014. Advantages of fluorescent microspheres compared with colloidal gold as a label in immunochromatographic lateral flow assays. Biosens. Bioelectron. 54, 262–265.
Yager, P., Edwards, T., Fu, E., Helton, K., Nelson, K., Tam, M.R., Weigl, B.H., 2006. Microfluidic diagnostic technologies for global public health. Nature 442 (7101), 412–418.
Yang, H., Li, D., He, R., Guo, Q., Wang, K., Zhang, X., Huang, P., Cui, D., 2010. A novel quantum dots-based point of care test for syphilis. Nanoscale Res. Lett. 5 (5), 875–881.
Yetisen, A.K., Akram, M.S., Lowe, C.R., 2013. Paper-based microfluidic point-of-care diagnostic devices. Lab Chip 13 (12), 2210–2251.
Yi, C., Li, C.-W., Ji, S., Yang, M., 2006. Microfluidics technology for manipulation and analysis of biological cells. Anal. Chim. Acta 560 (1), 1–23.
Zhang, X., Guo, Q., Cui, D., 2009. Recent advances in nanotechnology applied to biosensors. Sensors 9 (2), 1033–1053.
Zocco, A.T., You, H., Hagen, J.A., Steckl, A.J., 2014. Pentacene organic thin-film transistors on flexible paper and glass substrates. Nanotechnology 25 (9), 094005.